

Considerations of Thermodynamics and Kinetics for the Effects of Relative Humidity on the Electrolyte in Electrochemical Toxic Gas Sensors.

Michael L Hitchman ^{1*}, John R Saffell ²

1 Department of Pure and Applied Chemistry, University of Strathclyde, 295 Cathedral Street, Glasgow G1 1XL, UK
m.l.hitchman@strath.ac.uk

2 Alphasense Ltd, Sensor Technology House, 300 Avenue West, Skyline 120, Great Notley CM77 7AA, UK
john.saffell@alphasense.com

* Corresponding author: m.l.hitchman@strath.ac.uk

ABSTRACT: In this paper the physical chemistry of the absorption and desorption of water vapor for electrochemical gas sensors with commonly used sulfuric acid as the electrolyte is investigated. Electrochemical gas sensors are being increasingly used for monitoring toxic gases in the environment and they are, in principle, simple devices, but in practice their operation is complex. In particular, changes in atmospheric humidity and temperature can have significant effects on sensor output. A model has been developed for the calculation of sensor weight changes as humidity varies which are in good agreement with the analysis of experimental results. This then allows the calculation of the rather more important electrolyte volume variations. Changes in acid molarity and physical characteristics of the electrolyte have also been determined. The effects on working electrode (WE) electrocatalytic activity are discussed and potential problems with sensors for environmental monitoring are highlighted. In particular, changes in the electroactive area of the WE and, consequently, of the sensor output, and flooding of the WE catalyst aggregates which can lead to problems with electrolyte leakage from sensors are considered.

KEYWORDS: electrochemical gas sensors, air quality, relative humidity, electrolyte thermodynamics, water uptake, water evaporation, kinetic effects

Gas sensors are playing an ever-increasing role in environmental monitoring, medical and health applications, industrial and domestic safety, process control, smart city and smart building management, and security. Gas concentrations can be monitored using a range of sensing technologies, as discussed in the Supporting Information (SI).

Whatever the technique, though, the measurements made will be influenced by the local relative humidity (RH) of the environment, and an understanding of its effects is essential if accurate and meaningful results are to be obtained. In this paper we present the first detailed study of the humidity effects for amperometric toxic gas sensors by analysing the physicochemical behaviour of those sensors which allows us to explain experimental observations. In order to provide some background understanding we first briefly discuss sensor operation.

A schematic of an electrochemical gas sensor is shown in Figure S1, and an outline of the principles of its operation is given. In any electrochemical sensor, it is clear that the sensing or working electrode (WE) will not only be exposed to the analyte gas but also to the ambient gaseous environment that will include water vapor which

can adsorb onto the electrode catalyst and affect the electrochemistry. Such effects have been considered from the point of view of influences on sensor transient signals,¹ but, in addition, depending on the humidity level in the external atmosphere, water can be macroscopically absorbed by or desorbed from the electrolyte which will also affect the longer-term sensor operating characteristics. We will start by considering electrolyte effects.

Experimental and Observations of Weight Changes for Sensors Exposed to High RH

Two sets of experiments have been carried out. In the first set, Alphasense gas sensors for NO₂, H₂S and SO₂ in groups with varying numbers of sensor cells for each type were exposed without any external circuitry in a controlled environmental chamber (Climatec, custom built) at 50°C and with 90%RH. The sensors were of two form factors B and A types indicating, respectively, their overall diameters of 32 mm and 20 mm. The sensors are designated as NO₂-B1, NO₂-B2, NO₂-B3, NO₂-A1, NO₂-A2, H₂S-B1, H₂S-B2, H₂S-A1, and SO₂-B1. In addition, 1 cm³ of 5M H₂SO₄ in an open glass container with a diameter of ca 20 mm and a height of 32 mm was similarly exposed. Each sample was weighed at approximately daily intervals with minimum time outside of the chamber during weighing.

Figure 1 shows the % weight increases for batches for different types of sensor: - NO₂-B1, NO₂-A2, H₂S-B2, H₂S-A1, SO₂-B1 - and also for 5M H₂SO₄. Very similar plots were obtained for the other sensors listed above.

Before the samples were put into the environmental chamber they were stabilised at 22 ± 2°C and 23 ± 5 % RH over a saturated potassium acetate solution for two days. During stabilisation there were variations in % weight change which could be attributed to adjustments from earlier exposure of the acid electrolyte to variable lab atmospheric conditions. Thereafter there is a rapid weight rise for both the B and A-type sensors. However, between 13 and 16 days and between 27 and 29 days samples show falls in the % weight change. This occurred because they were taken out of the chamber and left in the lab environment as a result of technical issues with the chamber; all the plots recovered and continued the upward trend.

For both types of sensor, there are two sets of curves. For B type sensors the upper set in the plots were injected with a typical volume of 700 µL of acid and the lower set with 350 µL.² For A type sensors the corresponding electrolyte injection volumes were 350 µL and 175 µL. The weight increases of the sensors reach ~ 99% of the final value after varying times; this is discussed below.

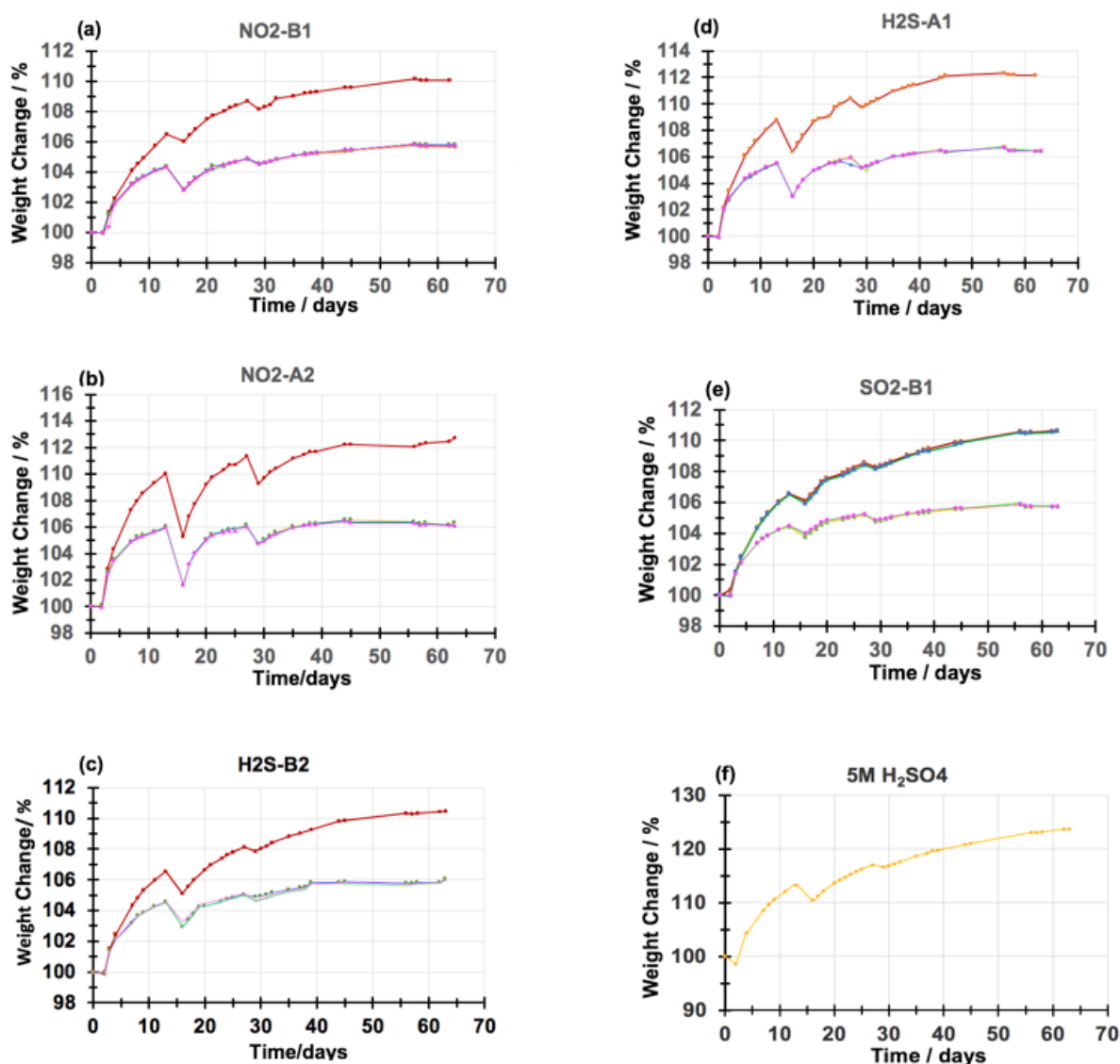


Figure 1. Percentage weight increases with time for sensors (a) NO₂-B1, (b) NO₂-A2, (c) H₂S-B2, (d) H₂S-A1, (e) SO₂-B1 and (f) 5M H₂SO₄ all exposed to 90%RH at 50°C

The second set of experiments was for H₂S-A2 sensors in 0%RH at 20°C. All the sensors were structurally identical except for the diameter of the gas entrance hole; cf. Figure S1. Figure 2 shows the weight loss as a function of time with the entrance hole diameters indicated.

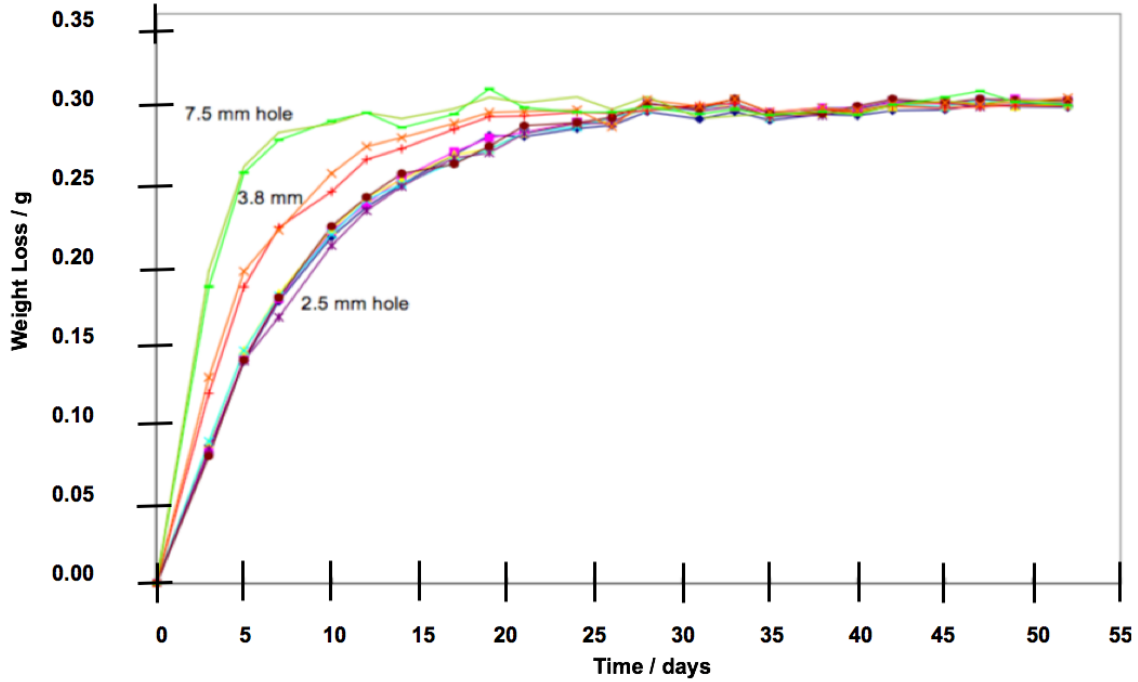


Figure 2. Weight loss for sensors H2S-A2 in 0%RH with different gas entrance hole diameters

We now consider the associated physical chemistry of sensor electrolytes.

Thermodynamic Aspects of Sensor Electrolytes

Partial Water Vapor Pressures

Water vapor pressure (p_w) as a function of thermodynamic temperature (T) is described by the Clausius-Clapeyron equation.³

$$d \ln p_w / dT = \Delta H_{vap} / RT^2 \quad (1)$$

where ΔH_{vap} is the enthalpy of vaporization. This equation can be integrated assuming that ΔH_{vap} is constant over the temperature range of integration and that the vapor phase behaves as an ideal gas:

$$\ln p_w = -\Delta H_{vap} / RT + \text{constant} \quad (2)$$

However, for water ΔH_{vap} does depend on the temperature and the vapor phase does not behave ideally. In the absence of exact theoretical equations, empirical equations are often used. The variation of the partial pressure of water over aqueous solutions of sulfuric acid (p_{wa}) has been described by Greenewalt⁴ with the following version of equation (2)

$$\log p_{wa} = -B/T + A \quad (3)$$

where A and B are constants (Table S1); note that this is in terms of Log base 10, and the gas constant R is included in B .

Table 1 gives partial pressure values calculated using the Greenewalt equation for fixed intervals of 10°C for the temperature range 0 to 50°C. Partial pressures of water (p_{wa}) over H₂SO₄ solutions have been calculated using equation (3); typically, in a sensor the H₂SO₄ is initially 5M, or 38.1 wt% and we have included this in both Table S1 and Table 1 by interpolating between 30% and 40%.

Table 1 Calculated partial pressures of water) over H₂SO₄ solutions using equation (3) and Table S1

Temp/°C	0	10	20	30	40	50
Temp/K	273	283	293	303	313	323
% H ₂ SO ₄	p_{ws} / kPa					
10	0.60	1.17	2.19	3.93	6.80	11.4
20	0.55	1.08	2.02	3.65	6.32	10.6
30	0.47	0.92	1.73	3.12	5.41	9.08
38	0.38	0.75	1.42	2.57	4.49	7.56
40	0.35	0.70	1.33	2.41	4.21	7.10
50	0.21	0.42	0.82	1.51	2.67	4.57
60	0.09	0.19	0.38	0.71	1.30	2.27
70	0.02	0.05	0.10	0.19	0.37	0.68
80	0.00	0.00	0.01	0.02	0.05	0.10
90	0.00	0.00	0.00	0.00	0.00	0.01
95	0.00	0.00	0.00	0.00	0.00	0.00

We should be aware that the values of A and B used to produce the partial pressures in Table 1 are accurate to $\pm 2\%$,⁴ so there will be some associated uncertainty in the values given in the table; we discuss this further below. We now look at how the partial pressures relate to %RH.

Considerations of Relative Humidity (RH) and Water Absorption

Introduction

RH is defined by the ratio of vapor partial pressure in the air (p_w) to the saturated vapor pressure (p_{ws}) (SVP) in air at the dry bulb temperature

$$RH \% = 100 \times p_w / p_{ws} \quad (4)$$

SVP is the vapor pressure at maximum content of water vapor in air before it begins to condense out as liquid water.

There are various published approximations for calculating the SVP over water and the equations are often quite complex with values varying by up to a few percent.^{5,6} Table S2 gives commonly accepted values of p_{ws} for the temperature range from 0° to 50°C; there will be some uncertainty associated with the p_{ws} values too.

The partial pressures of water (p_{wa}) over H₂SO₄ solutions (Table 1) will be for zero ambient RH so we can calculate the %RH that is generated by the water vapour pressure of the acid from 0°C to 50°C; it is simply $100 \times p_{wa} / p_{ws}$ – Table 2. The confidence intervals (CI) are calculated using standard statistics.

Table 2 Calculated %RH due to water vapour pressure over H₂SO₄

Temp / °C	0	10	20	30	40	50	
Temp / K	273	283	293	303	313	323	
% H ₂ SO ₄	%RH						Mean ± 95% CI
0	100.7	99.1	97.4	96.4	96.0	96.1	97.5 ± 1.2
10	96.7	95.1	93.6	92.6	92.1	92.2	93.7 ± 1.1
20	89.1	87.8	86.6	85.9	85.6	85.9	86.7 ± 0.8
30	76.0	75.0	74.0	73.4	73.3	73.5	74.2 ± 0.7
38	61.4	61.1	60.6	60.5	60.8	61.3	60.9 ± 0.2
40	57.3	57.0	56.7	56.7	57.0	57.5	57.0 ± 0.2
50	34.2	34.6	35.0	35.5	36.2	37.0	35.4 ± 0.6
60	14.9	15.5	16.1	16.8	17.6	18.4	16.6 ± 0.8
70	3.3	3.7	4.1	4.5	5.0	5.5	4.4 ± 0.5
80	0.3	0.4	0.5	0.6	0.7	0.8	0.5 ± 0.1
90	0.0	0.0	0.0	0.0	0.0	0.1	0.0 ± 0.0
95	0.0	0.0	0.0	0.0	0.0	0.0	0.0 ± 0.0

*Note: statistics are based on a larger data set

The lack of certainty about both p_{wa} and p_{ws} values will lead to uncertainties in %RH; again, this will be discussed later. Notwithstanding that comment, it is interesting to note the small variations in the absolute values of %RH with temperature for each acid concentration as indicated by the 95% confidence intervals. In the SI it is shown that there is no fundamental reason for the weakly dependent behaviour of RH with temperature and that it arises from the numerical values of the parameters in the derived equation for %RH.

Variations in Weight of H₂SO₄ Solutions with %RH

Because of the relatively weak dependence of %RH with temperature for any given value of the % concentration of H₂SO₄ we can plot the relationship between %H₂SO₄ and the average %RH with data from Table 2 - Figure 3. In general, ambient conditions are rarely below 10%RH, and we restrict the lower limit in the plot to > 5%RH.

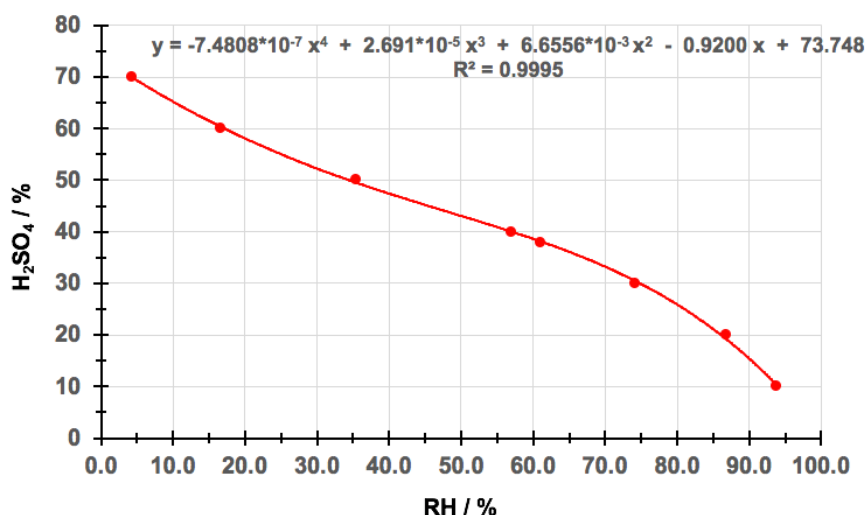


Figure 3 Plot of %H₂SO₄ as a function of atmospheric %RH

Using the polynomial equation in Figure 3 we can calculate the %H₂SO₄ concentrations for any value of %RH, starting with 1 g of 38% H₂SO₄ – Table 3.

Table 3 Values of H₂SO₄ concentrations related to %RH and weight changes on exposing 1 g of 38% H₂SO₄ solution to different %RH

%RH	%H ₂ SO ₄	Wt of water / g	Total New Wt / g
5	69	0.17	0.55
10	65	0.20	0.58
20	58	0.28	0.66
30	52	0.35	0.73
40	47	0.42	0.80
50	43	0.50	0.88
61	38	0.62	1.00
70	33	0.76	1.14
80	26	1.08	1.46
90	15	2.09	2.47
95	9	4.06	4.44

We can now examine the changes in weight of the electrolyte in a sensor when exposed to a humid atmosphere. We start with a solution of the 38% w/w (i.e. ~ 5M) H₂SO₄, with a total weight of the solution of 1 g so the solution will contain 0.38 g of acid and 0.62 g of water.

If the solution is left in air which has a %RH of, say, 80%, the acid solution will absorb water from the air until an equilibrium is reached and the acid has been diluted to 26% w/w - Column 2 in Table 3. Now, the same weight of acid, 0.38 g, is still present, but it is only constituting 26% of the total weight of the solution with the remaining 74% being water. Therefore, the weight of water absorbed will be $(0.38/26) \times 74 = 1.08$ g and the total weight of the solution will be 1.46 g – Columns 3 and 4, respectively in Table 3. The general formula for calculating the weight change on exposure of 38% acid to different values of %RH is:

$$\{0.38 / (\% \text{ H}_2\text{SO}_4 \text{ at the RH value})\} \times (100 - \% \text{ H}_2\text{SO}_4 \text{ at the RH value})$$

The calculation when 38% acid is equilibrated in air of a lower %RH, say 20%, is analogous. Water is lost until the acid strength increases to 58%, the weight of water left will be $(0.38/58) \times (100 - 58) = 0.28$ g, and the total weight of the solution will be 0.66 g – again, Columns 3 and 4, respectively. All the figures in Columns 3 and 4 correspond to an initial 1 g of acid solution. It can be noted that for 90%RH the ratio of the new weight to the initial weight is 2.47; i.e. the weight of the electrolyte has increased by a factor of 2.47. This is considered further in the following section.

Comparisons of Calculated Weight Changes with Experimental Results for Gas Sensors

The experimental plots shown in Figure 1 give a useful visual representation of the weight changes for sensors exposed to 90%RH. However, it is necessary to note that the measurements made of the initial weight (W_i) and at any other time (W_t) will be the sum of the weight of the sensor components (W_s) and the electrolyte (W_e).

Initially,

$$W_i = W_s + W_{ei} \quad (5)$$

and at time t

$$W_t = W_s + W_{et} \quad (6)$$

The ratio W_t / W_i clearly does not represent the ratio of the weight of the electrolyte at time t , W_{et} , to the initial electrolyte weight, W_{ei} , that we have calculated in Table 3.

As mentioned above, for a B-type sensor either 700 μL or 350 μL of 38% (5M) acid is injected. The density is 1.286 g cm^{-3} at 20°C (Figure S6); for the ambient weighing temperature of $\sim 22^\circ\text{C}$ there is only $\sim 0.1\%$ difference. Therefore, W_{ei} is either

$$W_{ei} = 1.286 \times 700 \times 10^{-3} = 0.900 \text{ g}$$

or

$$W_{ei} = 1.286 \times 350 \times 10^{-3} = 0.450 \text{ g}$$

Hence, knowing W_i we can readily determine the weight of the sensor, W_s , alone.

To illustrate the method we do this for sensors NO2-B3, with 700 μL of acid injection, which on day 2 had an average total weight W_i of 11.515 g. Thus, from equation (5)

$$W_s = 11.515 - 0.900 = 10.615 \text{ g}$$

Now, rearranging Equation (5) $W_{et} = W_i - W_s$

and with the value of W_t measured for day 63, for which the average was 12.817 g, then we obtain the equilibrium weight of the electrolyte ($W_{e,eq}$)

$$W_{e,eq} = 12.817 - 10.615 = 2.202 \text{ g}$$

Therefore, the ratio of the electrolyte weight at day 63 to the initial weight is

$$W_{e,eq} / W_{ei} = 2.202 / 0.900 = 2.45$$

This is within 1% of the calculated value given in Table 3 for 90%RH. A similar calculation obviously applies for an A-type sensor, except the volumes of electrolyte injected are 350 μL or 175 μL . Therefore, W_{ei} is either

$$W_{ei} = 1.286 \times 350 \times 10^{-3} = 0.450 \text{ g}$$

or

$$W_{ei} = 1.286 \times 175 \times 10^{-3} = 0.225 \text{ g}$$

And for, say, H2S-A1 it is found that the ratio $W_{e,eq} / W_{ei}$ with both volumes is 2.42, within 2% of the calculated value. So, from the measured total sensor weight data we can determine % weight changes for the electrolyte for B and A sensors with different initial acid injection volumes. Table 4 summarises the results.

For all the sensors and the acid alone, the overall average of the $W_{e,eq} / W_{ei}$ ratios is 2.45 ± 0.02 at the 95% confidence interval. The overall experimental average for the ratio is about 1% less than the calculated value of 2.47. This variance could arise from several sources:

- Uncertainties in the constants of Table S1 and in the resulting partial pressure of water (p_{wa}) over the sulfuric acid solutions (Table 1), and in the SVP of water (p_{ws}) (Table S2) would lead to associated lack of certainty in the %RH values (Table 2).
- Further approximations made when determining the variations in percentages of H_2SO_4 solutions with %RH (Figures 3 and S3).
- Small variabilities in the measured values arising from experimental imprecisions in weight and volume measurements and changeable environmental factors.

Table 4 Ratios of electrolyte weights initially and at 63 days

5M H ₂ SO ₄ Injected = 700 μL W _{ei} = 0.900 g						
Sensor	H2S-B1	NO2-B1	NO2-B2	NO2-B3	SO2-B1	H2S-B2
W _{e,eq} / W _{ei}	2.41	2.48	2.43	2.45	2.42	2.41
5M H ₂ SO ₄ Injected = 350 μL W _{ei} = 0.450 g						
Sensor	H2S-B1	NO2-B1	NO2-B2	NO2-B3	SO2-B1	H2S-B2
W _{e,eq} / W _{ei}	2.48	2.50	2.46	2.46	2.49	2.54
5M H ₂ SO ₄ Injected = 350 μL W _{ei} = 0.450 g						
Sensor		NO2-A1	NO2-A2	H2S-A1		
W _{e,eq} / W _{ei}		2.40	2.51	2.41		
5M H ₂ SO ₄ Injected = 175 μL W _{ei} = 0.225 g						
Sensor		NO2-A1	NO2-A2	H2S-A1		
W _{e,eq} / W _{ei}		2.42	2.52	2.42		
5M H ₂ SO ₄ Used = 1 mL W _{ei} = 1.286 g						
	5M H ₂ SO ₄					
W _{e,eq} / W _{ei}	2.51					

So taking all of that into account, the correlation between theory and experiment is remarkably good, and the analysis gives a quantitative understanding of the effect of humidity on sensor-electrolyte weight.

We can do a similar calculation for weight loss shown in Figure 2. At 0%RH and 20°C it can be seen from Table 2 that the sulfuric acid is, not unexpectedly, tending towards 100%. Extrapolating the Greenewalt parameters in Table S1 to 100% acid and calculating the partial pressure of water due to the acid shows it is found to be extremely low at 4.4×10^{-6} kPa. So with 0%RH the approximately 0.3 g of weight loss seen in Figure 2 will be all of the water from the acid which will correspond to the 62% in the starting electrolyte of 38% w/w acid. Therefore, the ratio of the electrolyte weight at equilibrium after about 30 days to that initially will be $0.18/0.48 = 0.38$.

Entering an additional row with 100% H₂SO₄ in column 2 in Table 3 and using the same procedure for calculating the weight of water as for the other acid concentrations gives a total new weight of 0.38 g, as measured.

Weight changes can be easily and exactly measured, but they are not of direct interest in considering sensor operation. Electrolyte volume changes cannot be readily determined, but they are much more important, as discussed in the section after the next. Before looking at volume changes, though, we examine the nature of the weight variation with time.

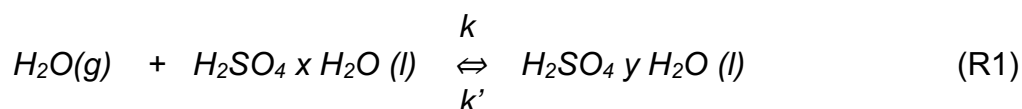
Kinetics of the Time Dependence of Sensor Weight Changes

Describing the rate of water evaporation from the liquid phase to the vapor phase and of the converse condensation is not straightforward and there are a number of approaches. One is based on boundary layer theory⁷ and another on gas kinetics,⁸ but in those models just water is considered and only for its evaporation. The evaporation and condensation of water has also been considered.⁹ However, they are all only concerned with what is happening at the interface between the two phases. In our case of sulfuric acid electrolyte in a sensor, changes in the water content involve changes in the hydration of the acid, and it requires those changes to permeate throughout the entire liquid volume of the sensor. Furthermore, the situation will be complicated by the concentration of the acid varying with depth in the sensor and with time. In addition, the ease with which water molecules will be released from or absorbed by the solution will be influenced by chemical factors such as hydrogen bonding. As is well known, the unusual properties of liquid water are attributed to

hydrogen bonding.¹⁰ For sulfuric acid solutions hydrogen bonding is also present, but it is rather more complex since there can be up to 7 hydrates, $H_2SO_4 \cdot nH_2O$ which will undoubtedly affect the evaporation and condensation of water.¹¹

If we now consider the permeation just mentioned, that will require diffusion of water vapor to and from the gas entrance of the sensor, through the porous PTFE, and then through the layers of electrolyte to the counter electrode (CE); cf. Figure S1. That is a planar multilayer diffusion problem involving Fickian and Knudsen diffusion in the gas phase, and solution diffusion in the electrolyte.¹² For each layer there will be an individual mass transfer coefficient and we could examine the individual diffusional transport through each one. However, that would only take into account unidirectional flow. A theoretical analysis on that basis has been made, but it does not replicate the observed approach to equilibrium.²

To deal with the overall reality of the situation, a combination of condensation and evaporation occurring simultaneously for a fixed temperature and a constant presence of a fixed humidity should be considered. The interaction between the water vapor and the electrolyte has to be represented by a reversible process; e.g.



where $H_2O(g)$ is water vapor, $H_2SO_4 \cdot x H_2O(l)$ is hydrated acid electrolyte, and $H_2SO_4 \cdot y H_2O(l)$ is more heavily hydrated acid. The water vapor being continuously supplied in the environmental chamber will not be depleted, and so the reaction is pseudo-first order with rate constants k and k' for the forward and reverse processes. Using the weight symbols used earlier the relationship of the amounts of the electrolyte being hydrated at time t , W_{et} , to the value initially, W_{ei} , and to that at equilibrium, $W_{e,eq}$, is given by¹³

$$\ln \frac{W_{ei} - W_{e,eq}}{W_{et} - W_{e,eq}} = (k + k')t \quad (7)$$

The effective rate constant is the sum of the individual rate constants.

Since, as we shall see, the rate constant for that reaction is low at $\sim 0.1 \text{ day}^{-1}$ (Table 5), then for any given short measurement time there will be an effective steady state and the weight will be W_{et} ; note that since the argument of the \ln term consists of weight differences we can take the total weights and the sensor weight is removed from the calculation.

However, in order to meaningfully plot data from Figure 1 and for other sensors we must consider the times where the sensors were taken out of the environmental chamber as mentioned earlier. That happened on two occasions, after 13 days and after 27 days. Taking those time intervals out of the data sets can, in principle, allow equation (7) to be tested. A typical plot for NO₂-B1 with 700 μL of acid has a good fit up to 45 days with $R^2 = 0.992$.

For other sensors, though, the recovery after removal from the environmental chamber shows some variability, and there are significant differences in the quality of the plots. The data uncertainties in the recovery of the weight increases can, however, be overcome by simply taking the data up to the first time of 13 days when the sensors were first removed from the chamber. Figure 4 shows examples of plots of equation (7) for A and B type sensors, for 3 different sensor types, and for different electrolyte

volumes. In all cases the plots are very good fits to the data. Table 5 summarizes the slopes for all the sensors.

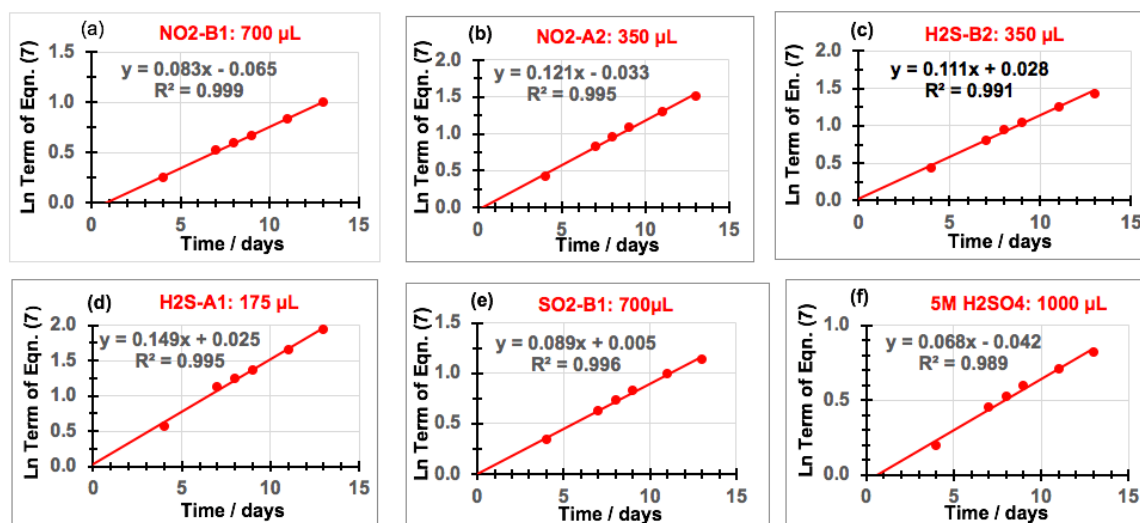


Figure 4 Examples of plots of equation (7) for data for five sensors types and H_2SO_4 with acid volumes given: (a) NO2-B1; (b) NO2-A2; (c) H2S-B2; (d) H2S-A1; (e) SO2-B1; (f) H_2SO_4

Table 5 Summary of the kinetic rate constants (days^{-1}) from the slopes of the plots with weight gains for equation (7)

Sensor	Acid Volume / μL	
	350	700
NO2-B1	0.112	0.083
NO2-B2	0.142	0.088
NO2-B3	0.198	0.106
	350	700
H2S-B1	0.122	0.080
H2S-B2	0.111	0.086
SO2-B1	0.117	0.089
	175	350
NO2-A1	0.199	0.118
NO2-A2	0.277	0.121
H2S-A1	0.149	0.096
	1000	
H_2SO_4	0.068	

There are some interesting observations that can be made about the values of the slopes for the kinetic plots. First it can be seen that for each batch of sensors the rate constants are always lower for the larger volume of electrolyte; the ratio of the slopes for all the sensors, apart from NO2-A2, is about 1.5. With larger volumes the acid will occupy a greater depth in the electrolyte reservoirs. That will mean that for water diffusing through the electrolyte stack, according to the Einstein-Smoluchowski equation,³ it will take longer for that to occur:

$$t = d^2 / 2D \quad (8)$$

where t is the time for diffusion, d is the electrolyte depth in the reservoir, and D is the water diffusion coefficient. For H_2SO_4 in the beaker the depth will be even greater; initially it will be ~ 3 mm, and hence it has the smallest rate constant.

Clearly, sensor construction could have an effect on the kinetics of the humidification, and that could apply to structural features including hole diameter, filters and working electrode materials; the variation in the slopes will reflect that. The very high slope value for sensor NO2-A2 with 175 μL is anomalous and is not understood.

The effect of hole diameter has been shown in Figure 2. Before considering that we apply the same analysis to the three data plots in Figure 2. Plots of equation (7) are again good fits to the data ($R^2 > 0.99$) and since there was no interruption in the measurements, the analysis can be taken close to the final weight loss. However, because of variations in the data and resulting errors introduced in the difference terms in the argument of the Ln , the analysis cannot be usefully extended beyond about 95% of the final weight loss. It is interesting to note that a plot of data from Figure 2 of hole diameter ratios as a function of the slope ratios for equation (7) obtained from the three hole diameters indicated in Figure 2 has a slope of 1.01 with $R^2 = 0.998$.

Whenever a gas interacts with the surface of a condensed phase, as in reaction (R1), the mass flow, in terms of weight loss or gain, is described by a mass diffusional flux, j ($\text{mol cm}^{-2}\text{s}^{-1}$). For flow of the gas itself, as through the entrance hole, the diffusional process is described by volumetric flow, v ($\text{mol cm}^{-3}\text{s}^{-1}$). The two mass flows must be the same and to remain dimensionally homogeneous a proportionality constant with units of length is required. The characteristic length of the different cylindrical tubes is the hole diameter, d , and so $j = d \times v$, and the weight change is proportional to the hole diameter.

Another aspect of the kinetics comes from treating humidification as a pseudo-first order process. Expressing the combined rate constant ($k + k'$) in equation (7) as k'' , the half-life ($t_{1/2}$) will be given by

$$t_{1/2} = \text{Ln } 2 / k'' \quad (9)$$

The kinetic rate constants in Table 5 will all give half-lives less than the disturbance at 13 days, and when calculated and measured values are compared there is good agreement. For example, with H2S-A1 the half-lives from Table 5 are 4.7 and 7.2 days and the measured values are 5 and 7 days.

For the weight loss data (Figure 2) the calculated and measured half-lives agree exactly: 2.0 d, 3.6 d, and 5.0 d for the entrance hole diameters of 7.5 mm, 3.8 mm, and 2.5 mm, respectively.

The usefulness of half-lives is that by considering 5 or 6 half-lives the time for equilibrium of water vapor transfer can be obtained.

Variations in Volume of H_2SO_4 Solutions with %RH

As noted above, although electrolyte volume changes are much more important than weight changes, they cannot be readily determined. Here we calculate the volume changes of the acid solutions, but we will need the values of density for different % H_2SO_4 solutions as a function of temperature. Figure S6 shows these and the fitted quadratic equations give calculated density values in agreement with published data to better than $\pm 0.5\%$.

From Table 3 we have the % acid concentrations for stepped %RH values, and the corresponding new weights; these are reproduced in Table 6 – columns 2 and 3. From the quadratic equations given in Figure S6 we can calculate the corresponding solution densities – columns 4, 7 and 10. Now with the actual values of solution

weights from Table 6 – column 3 – we can calculate the corresponding solution volumes – columns 5, 8 and 11. Columns 6, 9 and 12 give the ratios of the new volumes to the initial volume for 38% H₂SO₄.

The ratios of new volumes to original volumes can be used to calculate volume changes for different starting weights of electrolyte; the expected weak temperature dependence can be seen. From the % H₂SO₄ values and the solution volumes the solution molarities can be calculated – Table 7.

The large changes in acidity could have dramatic effects on WE electrocatalytic activity, and the extensive range of electrolyte molarities could mean that significant variations with %RH could affect sensor sensitivity, the influence of interferents, and reproducibility. We consider this in the next section.

Table 6 Values of H₂SO₄ concentrations related to %RH and volume changes on exposing 1 g of 38% H₂SO₄ solution to different %RH

%RH	% H ₂ SO ₄	Total New Wt / g	0°C			20°C			50°C		
			Density/ g cm ⁻³	Vol / cm ³	New V / Initial V	Density/ g cm ⁻³	Vol / cm ³	New V / Initial V	Density/ g cm ⁻³	Vol / cm ³	New V / Initial V
5	69	0.55	1.610	0.34	0.44	1.598	0.34	0.44	1.572	0.35	0.44
10	65	0.58	1.563	0.37	0.48	1.551	0.37	0.48	1.525	0.38	0.48
20	58	0.66	1.489	0.44	0.58	1.477	0.45	0.57	1.452	0.45	0.58
30	52	0.73	1.429	0.51	0.66	1.418	0.51	0.66	1.393	0.52	0.66
40	47	0.80	1.380	0.58	0.75	1.369	0.58	0.75	1.345	0.59	0.75
50	43	0.88	1.341	0.66	0.85	1.331	0.66	0.85	1.308	0.67	0.85
61	38	1.00	1.298	0.77	1.00	1.289	0.78	0.99	1.267	0.79	1.00
70	33	1.14	1.250	0.91	1.18	1.242	0.92	1.18	1.221	0.93	1.18
80	26	1.46	1.191	1.23	1.59	1.184	1.23	1.58	1.165	1.25	1.59
90	15	2.47	1.104	2.24	2.90	1.101	2.24	2.88	1.085	2.28	2.88
95	9	4.44	1.061	4.19	5.44	1.060	4.19	5.37	1.045	4.25	5.38

Table 7 Molarity related to volume changes on exposing 1 g of 38% H₂SO₄ solution to different %RH at 20°C

%RH	% H ₂ SO ₄	Vol / cm ³	Molarity
5	69	0.34	11.4
10	65	0.37	10.5
20	58	0.45	8.6
30	52	0.51	7.6
40	47	0.58	6.7
50	43	0.66	5.9
61	38	0.78	5.0
70	33	0.92	4.2
80	26	1.23	3.2
90	15	2.24	1.7
95	9	4.19	0.9

Effects of Relative Humidity on Sensor Characteristics and Performance

Electrolyte Changes

The effect of humidity on gas sensors has been analysed in terms of changes in the electrolyte weight, volume and molarity for all of the electrolyte in the sensors and these have been seen to occur over many days. In addition, though, there will be changes taking place in the local electrode vicinity. The most obvious effect will be on the electrolyte composition at an electrode surface where there is a three-phase interface, as indicated in Figure S2. Changes at that interface will be largely controlled by the slowest of the mass transfer processes of binary diffusion of water vapor in air, and water diffusion in the electrolyte film over the WE, which is shown in the third

section in the SI to be the diffusion in the electrolyte. The electrolyte film in a gas porous membrane typically has a thickness of $\sim 1 \mu\text{m}$,¹⁴ and with a diffusion coefficient of $\sim 10^{-5} \text{ cm}^2\text{s}^{-1}$ the time to change the acid concentration in the film will be only ~ 1 ms; cf equation (8). It is also shown in that section of the SI that changes in electrolyte composition can affect the level of wetting on the walls of the membrane pores giving variations of electroactive area and of sensor output. Electrolyte volume changes can also produce flooding of the WE catalyst aggregates which can lead to problems with electrolyte leakage from sensors.

The composition changes at the three-phase interface will, though, be the same as in the bulk, and from Table 7 it can be seen that the molarity will vary from $\sim 11.4\text{M}$ at 5%RH to $\sim 0.9\text{M}$ at 95%RH. Considerations of the dissociation of H_2SO_4 show that sulfuric acid behaves like a 1:1 electrolyte (e.g. HCl) over the molarity range from 1 to 14M,¹⁵ so the proton molarity in the sensor will vary from ~ 1 to $\sim 11\text{M}$. Of course, activities should be used instead of concentrations; values of activity coefficients are available.¹⁶ The changes in molecular and proton molarity could be expected to influence the electrochemistry of sensor processes and we discuss that in the next section.

Electrochemistry

We now consider two electrochemical processes involving toxic gases where general effects of acidity on I-V features have been investigated. First let us look at CO oxidation. Figure. 5 shows typical I-V curves obtained with a CO gas sensor when exposed to air and 400 ppm CO in air for a bias potential with respect to the internal high surface area Pt (Pt HSA) reference electrode (RE).

There is activation control at low currents and a well-defined mass transport controlled current plateau for the oxidation of CO at the Pt HSA WE.

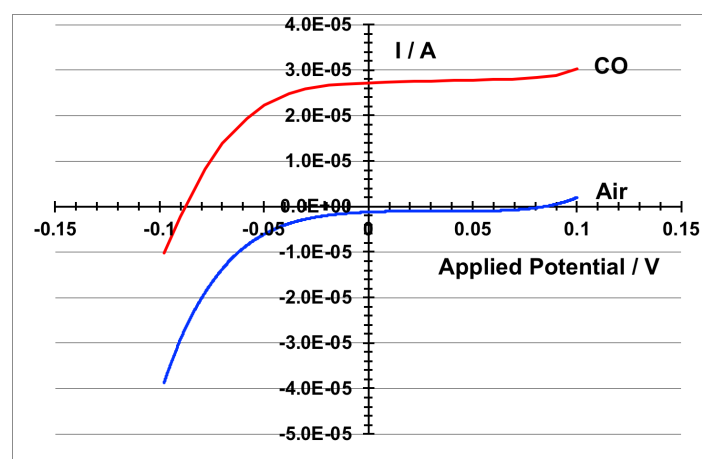


Figure 5 I-V curves obtained for 400 ppm CO in air and for air at the WE of a CO sensor

A study of CO electro-oxidation on porous Pt-Ru electrodes in sulfuric acid electrolytes of 0.5M, 1.0M, 2.5M and 4.0M has shown an anodic voltage shift in the kinetically activated region of the I-V curves of about 0.2 V between the lowest and highest acid molarities; there is a reasonably linear correlation between the two.¹⁷ The rate determining step for the oxidation appears to involve a surface reaction between CO and OH adsorbed species so similar behaviour might be expected with a Pt electrocatalyst in the kinetically controlled region (ca. -0.05 V to -0.09V in Figure 5) for

a CO sensor. If we then consider a %RH change from, say, 95% to 70% with a molarity increase from 0.9M to 4.2M (Table 7) this would shift the I-V curve anodically by about 190 mV, and CO oxidation would no longer be occurring with a mass transport controlled current at a zero-bias potential (ZBP). Conversely, changes to higher %RH, say from 30% to 70% with a molarity change from 7.6M to 4.2M, could move the I-V curve cathodically by 200 mV; that assumes that the potential shift reported above continues to be linearly dependent on the acid molarity at concentrations higher than 4M. The observations are consistent with the finding that there is a potential independent reaction order of -1 for the rate of CO oxidation with respect to $[H^+]$; in other words, as the $[H^+]$ increases the oxidation current will decrease and a more anodic applied potential would be needed to maintain the CO electro-oxidation.

That discussion of CO oxidation is all in terms of the kinetic processes, but we need to look at the thermodynamics as well. As noted above, the WE is at ZBP with respect to the internal RE. Our measurements of the electrode potentials show the electrodes are at $\sim +840$ mV vs SHE. The equilibrium (R2) for the WE



indicates that acid molarity will affect the value of the ZBP for the electro-oxidation.¹⁸ However, the overpotential associated with the applied potential +0.84 V will not be greatly affected by variations in the proton activity since in order to calculate the equilibrium potential with the Nernst equation, $[H^+]$ is in a Ln term which will minimize its influence; that will be true even if activities are used instead of concentrations.

The equilibrium associated with the RE is usually attributed to the O_2/H_2O couple (R3); the rationale for that is discussed below.



That process will also not be disturbed unduly by $[H^+]$ changes.

Therefore, although the thermodynamics of the system will not lead to any significant measurement problems for CO, it is apparent that there needs to be careful consideration of sensor operation arising from process kinetics for CO electro-oxidation when there are changes in environmental RH. And even though the effect of acid molarity interaction on CO kinetics arises from surface reaction of adsorbed CO, similar effects may occur with other toxic gas sensors using Pt, or similar materials, as WE electrocatalysts.

One also needs to consider the effect of changes in acid molarity on the base line current which is generally regarded as having a contribution from the reduction of aerial oxygen. To justify that requires the determination of the overpotential of the WE with respect to the internal RE. We just illustrate the procedure here.

The overpotential (η) by definition is the difference between the applied potential (E_{app}) and the equilibrium potential (E_{eq}) for the RE process. For equilibrium (R3), E_{eq} is described by the Nernst equation

$$E_{eq} = E^0 + 2.303 (RT/4F) \log pO_2 \times [H^+]^4 \quad (10)$$

For the argument of the log term we replace pO_2 by $[O_2]$ since the gas solubility changes with acid molarity because of the salting-out effect;¹⁹ the saturation concentrations of dissolved oxygen in highly acidic aqueous solutions of H_2SO_4 have been published by Das.²⁰ The proton concentrations also need to be substituted by proton activities, as mentioned earlier. That is all relatively straightforward, and, as noted, the value of the overpotential will not be unduly affected because of the insensitivity of the log term on the magnitudes of the components of the argument. There is a problem, though, in knowing what the value of E^0 in equation (10) should be. The value of +1.23 V is obtained by thermodynamic calculations, but this value is rarely determined experimentally. The difficulty in attaining the potential has been

attributed to a number of causes, in particular the nature of the electrode, the possibility of the formation of hydrogen peroxide, the effect of layers of oxygen adsorbed on the surface,²¹ and the interference of currents from low level impurities in the solution.²² The measured equilibrium potential can be found to be many millivolts cathodic of +1.23 V and so the extent of an oxygen reduction would be greatly diminished. However, it can be shown that even if it is assumed that in the unlikely event the empirical value of E^0 is as much as 800 mV cathodic of the thermodynamic value, η is still sufficiently cathodic for O₂ reduction to occur, so it is not unreasonable to attribute some of the background current to that process.

Finally, we should consider that if the I-V curve for the CO is being shifted by changes in the acid molarity, whether the same is happening for the background current. Unfortunately, we have not found any studies of that. If there is a similar effect to that for the I-V curves for CO it is unlikely to match the voltage shifts for those curves so one would not be able to reliably correct the analytical currents for the background contributions. Again, the effects of changes in environmental RH on the process kinetics for CO electro-oxidation is emphasized. We now look at the case for NO₂ sensors.

Figure 6 shows typical I-V curves that we have obtained for 2 ppm NO₂ in air and for air with a carbon based WE.

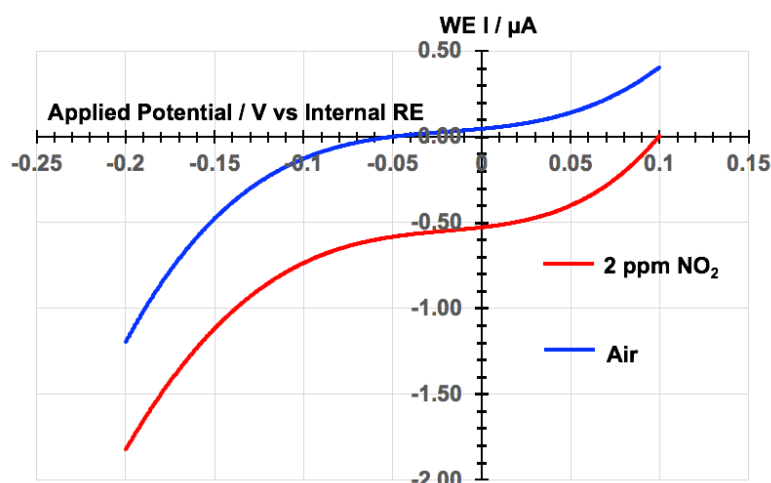
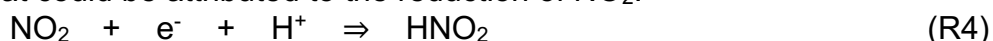


Figure 6 I-V curves for obtained in air and for 2 ppm NO₂ in air with a carbon-based electrode

There is a mass transport-controlled region around a ZBP. It has been suggested that could be attributed to the reduction of NO₂.²³



One would expect any changes in electrolyte acidity to have an effect on the sensor performance and a study of the effect of acid strength on NO₂ reduction on edge plane pyrolytic graphite (EPPG) using cyclic voltammetry supports that.²³ That study has found that with 0.1 M acid no reduction wave was observed in the cyclic voltammogram, and for 1.0 M acid the reduction wave was also absent; in both cases, though, oxidation waves were present. However, with 2.5 M acid, a quasi-reversible redox couple was evident with both a reduction wave and oxidation waves.

Clearly, the effect of pH on the reduction of NO₂ is complex and there will be an influence of dilution of the electrolyte on sensor characteristics. It has to be noted, though, that the results discussed above are for EPPG which could well have different characteristics from the carbon-based electrode used to obtain the results shown in Figure 6. Table 7 shows that with 85%RH the acid molarity will be ~ 2.5M so NO₂

reduction could occur. And since no results are given in reference 23 for EPPG in 1 M < acid < 2.5M, NO₂ reduction could still be occurring for up to 90%RH. That is in line with the usual humidity specification for operation between 15 and 90%RH, and with what is found in practice for NO₂ sensors. Nevertheless, as for CO sensors, caution is needed as the %RH varies.

Conclusions

We have reported on the weight changes observed when electrochemical toxic gas sensors have been exposed to 90% and 0% RH. An analysis of the thermodynamics of water absorption and desorption has been made and the calculated weight changes are in good agreement with the experimental results. It also provides a rationale for the low temperature dependence of the equilibrium RH of sulfuric acid.

The kinetics of the time dependence of the weight changes have been analysed in terms of a reversible equilibrium for water evaporation and condensation and the kinetic plots are very good fits to the data. The kinetic model also provides some understanding of the dynamic process of mass flow to and from the sensors.

The thermodynamic approach allows the calculation of the volume changes of the acid solutions in the sensors, and the results can be generalised to allow the volume calculations for different starting weights of electrolyte. From the volume changes the resulting variations in acid molarity can be determined.

The effects of molarity changes on sensor characteristics and performance have been discussed for two types of toxic gas sensors, CO and NO₂. For CO sensors published results on voltage shifts in I-V curves induced by changes in acid molarity have been discussed and it is apparent that caution is needed when variations in %RH lead to such changes. Effects on the thermodynamics of the CO system and the associated background currents in relation to the environmental RH are shown to be less concerning.

For NO₂ sensors, again the effect of humidity is complex and there will undoubtedly be an influence of dilution of the electrolyte on sensor characteristics. However, the indications are that sensors can be used with up to 90%RH without undue compromise of sensor performance, and it may be possible to operate satisfactorily up to 95%RH. Nevertheless, as for CO sensors, caution is needed as the %RH varies.

The discussions about the influence of humidity changes on sensor operation indicate the uncertainties there are for how sensor electrochemistry can be affected by changes in electrolyte pH. As mentioned in the introduction to this paper, all sensors will be influenced by the local environmental RH. It is surprising therefore that there have been so few studies of the issue. This paper has provided a quantitative analysis of one aspect of those matters, but much more needs to be done to obtain a deeper understanding of electrochemical gas sensor characteristics.

ASSOCIATED CONTENT

The Supporting Information (SI) is available free of charge.

The SI consists of a schematic of sensor structure and an outline of sensor operation; tables of thermodynamic parameters; considerations of the effect of RH changes on electrolyte in the microporous PTFE membranes; temperature dependence of %RH

for H₂SO₄ solutions; densities for different % H₂SO₄ solutions as a function of temperature

AUTHOR INFORMATION

Corresponding Author

Michael L. Hitchman – Department of Pure and Applied Chemistry, University of Strathclyde, 295 Cathedral Street, Glasgow G1 1XL, UK
Email: m.l.hitchman@strath.ac.uk

Authors

Michael L. Hitchman – University of Strathclyde G1 1XL, UK
John R Saffell – Alphasense Ltd, CM77 7AA, UK

Notes

MLH has no competing interests, and JRS is CTO of Alphasense Ltd.

Acknowledgements

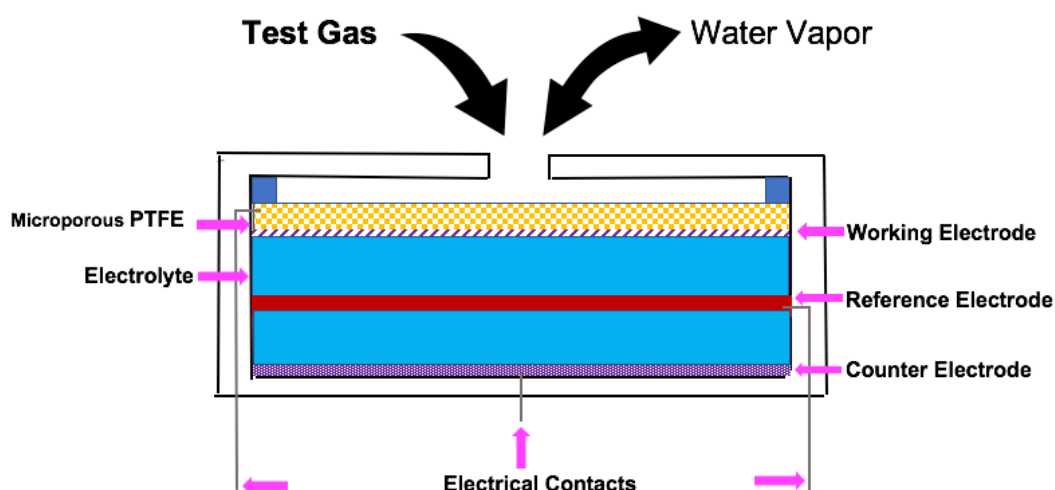
The authors thank Gosia Janiuk for assistance with the weight measurements and Dr Brian McMillan for producing the current voltage curves.

REFERENCES

- (1) Farquhar, A.K.; Henshaw, G.S.; Williams, D.E. Understanding and correcting unwanted influences on the signal from electrochemical gas sensors. *ACS Sens.* **2021**, *6*, 1295-1304.
- (2) Chan-Henry, R.Y. Design and development of electrochemical gas sensors, *PhD Thesis*, City University London, **1992**.
- (3) Atkins, P.W. *Physical Chemistry*, 4th ed., OUP: Oxford, **1990**, Ch. 6.
- (4) Greenewalt, C.H. Partial pressure of water out of aqueous solutions of sulfuric acid. *Ind & Eng Chem.* **1925**, *17*, 522-523.
- (5) Huang, J. A simple accurate formula for calculating saturation vapor pressure of water and ice. *J. Appl. Meteor. Climatol.* **2018**, *57*, 1265–1272. (b) https://en.wikipedia.org/wiki/Vapour_pressure_of_water.
- (6) Lide, D.R. (ed.) Vapor pressure of water and other saturation properties of water. *CRC Handbook of Chemistry and Physics, 90th ed.; Internet Version*. CRC Press: Boca Raton, **2010**, p. 6–5.
- (7) Hisatake, K.; Fukuda, M.; Kimura, J.; Maeda, M.; Fukuda, Y. Experimental and theoretical study of evaporation of water in a vessel, *J Appl. Physics*, 1995, *77*, 6664-6674.
- (8) Eames, I.W.; Marr, N.J.; Sabir, H. The evaporation coefficient of water: a review, *Int. J. Heat Mass Transfer*, **1997**, *40*, 2963-2973.
- (9) Vlasov, V.A. Modeling of evaporation and condensation processes: a chemical kinetics approach. *Heat and Mass Transfer*, **2019**, *55*, 1661–1669.
- (10) Silverstein, K.A.T.; Haymet, A.D.J.; Dill, K.A. The strength of hydrogen bonds in liquid water and around nonpolar solutes, *J. Am. Chem. Soc.* **2000**, *122*, 8037-8041.
- (11) Bandy, A.R.; Ianni, J.C. Study of the hydrates of H₂SO₄ using density functional theory. *J. Phys. Chem. A.* **1998**, *102*, 6533-6539.
- (12) Hitchman, M.L.; Cade, N.J.; Gibbs, T.K.; Hedley, N.J.M. Study of the factors affecting mass transport in electrochemical gas sensors, *Analyst*, **1997**, *122*, 1411-1417.

- (13) Frost, A.A.; Pearson, R.G. *Kinetics and Mechanism*, 4th ed.; Wiley: New York, **1965**.
- (14) Liebhafsky, H.A.; Cairns, E.J. *Fuel Cells and Fuel Batteries*, Wiley: New York, **1968**.
- (15) Robinson, R.A.; Stokes, R.H. *Electrolyte Solutions*, Butterworths, London, **1970**.
- (16) Harned, H.S.; Hamer, W.J. The thermodynamics of aqueous sulfuric acid solutions from electromotive force measurements. *J. Am. Chem. Soc.* **1935**, *57*, 27-33.
- (17) Arico, A.S.; Modica, E.; Passalacqua, E.; Antonucci, V.; Antonucci, P.L. Carbon monoxide electrooxidation on porous Pt-Ru electrodes in sulfuric acid. *J. Appl. Electrochem.* **1997**, *27*, 1275-1282.
- (18) Kortlever, R.; Shen, J.; Schouten, K.J.P.; Calle-Vallejo, F.; Koper, M.T.M. Catalysts and Reaction Pathways for the electrochemical reduction of carbon dioxide. *J. Phys. Chem. Letts.* **2015**, *6*, 4073-4082.
- (19) Hitchman, M.L. *Measurement of Dissolved Oxygen*, Wiley: New York, **1978**.
- (20) Das, T.N. Saturation concentration of dissolved O₂ in highly acidic aqueous solutions of H₂SO₄. *Ind. Eng. Chem. Res.* **2005**, *44*, 1660-1664.
- (21) Bagotskii, V.S.; Nekrasov, L.N.; Shumilova, N.A. Electrochemical reduction of oxygen. *Russian Chemical Reviews*, **1965**, *34*, 717-730.
- (22) Bockris, J.O'M.; Reddy, A.K.N. *Modern Electrochemistry, Vol. 2*, Plenum Press: New York, **1973**.
- (23) Banks, C.E.; Goodwin, A. Heald, C.G.R.; Compton, R.G. Exploration of gas sensing possibilities with edge plane pyrolytic graphite electrodes: nitrogen dioxide detection. *Analyst*, **2005**, *130*, 280-282.

For TOC Only:



Supporting Information

Considerations of Thermodynamics and Kinetics for the Effects of Relative Humidity on the Electrolyte in Electrochemical Toxic Gas Sensors.

Michael L Hitchman ^{1*} and John R Saffell ²

- 1 Department of Pure and Applied Chemistry, University of Strathclyde, 295 Cathedral Street, Glasgow G1 1XL, UK
m.l.hitchman@strath.ac.uk
- 2 Alphasense Ltd, Sensor Technology House, 300 Avenue West, Skyline 120, Great Notley CM77 7AA, UK
john.saffell@alphasense.com

Corresponding Author: m.l.hitchman@strath.ac.uk

Contents

Gas sensor technologies with a schematic of electrochemical gas sensor structure and an outline of sensor operation

Thermodynamic parameters

Considerations of the effect of %RH changes on electrolyte in the microporous PTFE membranes

Temperature dependence of %RH for H₂SO₄ Solutions

Densities for different %H₂SO₄ solutions as a function of temperature

Gas sensor technologies with a schematic of electrochemical gas sensor structure and an outline of sensor operation

Sensor technologies for monitoring gas concentrations include:

- resistance and semiconductor properties of metal oxides
- capacitance of films between two electrodes
- resonant frequency in a solid generated by an acoustic wave
- temperature increase generated by phase change or chemical reaction
- optical properties such as absorbance, emission, interference and refractive index determined by UV, IR and Raman spectroscopy, luminescence phosphorescence, and fluorescence
- electrochemical currents and voltages

Figure S1 is a schematic diagram of the structure of an amperometric gas sensor with axisymmetric geometry.

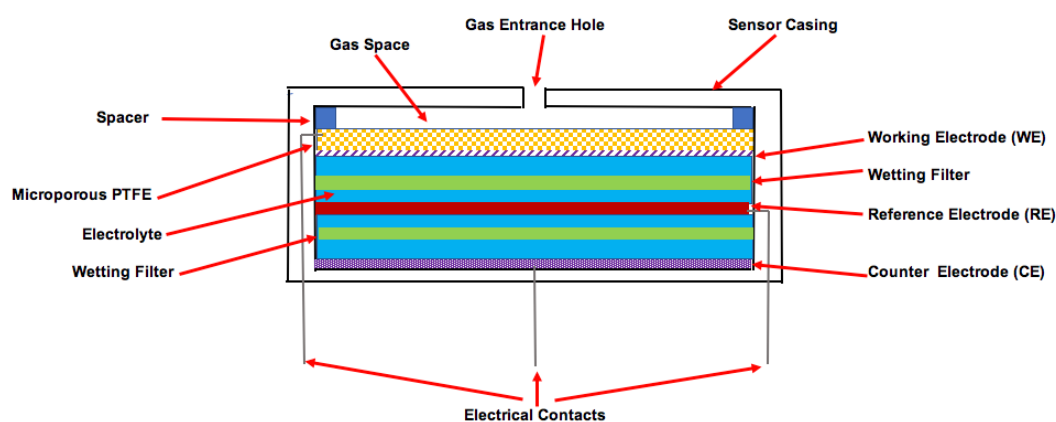


Figure S1 Schematic of a membrane covered amperometric gas

The rate of the analyte gas entering the sensor is controlled by the entrance hole and it distributes over the total area of the gas space. The gas then diffuses into the gas porous PTFE membrane and contacts the interpenetrating electrolyte and the sensing, or working electrode (WE) that is in intimate contact with the underside of the gas porous membrane; a more detailed description of the three-phase interface of gas, liquid and solid is given below in the section after next. The electrocatalyst in the WE is chosen according to the analyte gas being monitored. The other two electrodes in the cell, the counter electrode (CE) and the reference electrode (RE), often have a similar chemical composition to the WE catalyst; all three electrodes are usually stacked parallel to each other, as illustrated in Figure S1. The cell electrolyte, which is frequently sulfuric acid with a molarity of 3 to 7M, provides ionic electrical contact between the electrodes, usually with the aid of hydrophilic separators, labelled “wetting filters” in Figure S1, to provide capillary transport. A potentiostatic circuit maintains the potential of the WE at a fixed value with respect to the RE potential to allow the analyte gas to be reduced or oxidized. The RE needs to provide a stable potential to ensure that the WE is always anchored in the correct potential region of the current-voltage curve to maintain a constant sensitivity and to minimise reaction with interfering gases. The CE completes the current flow in the external circuit and generates an equivalent current in the opposite sense to that of the WE.

Thermodynamic parameters

Table S1 Parameters for equation (3)¹

% H ₂ SO ₄	10	20	30	35	38	40	45	50	55
A	8.925	8.922	8.864	8.873	8.852	8.844	8.809	8.832	8.827
B	2259	2268	2271	2286	2293	2299	2322	2357	2400
% H ₂ SO ₄	60	65	70	75	80	85	90	95	
A	8.841	8.853	9.032	9.034	9.293	9.239	9.255	9.790	
B	2458	2533	2688	2810	3040	3175	3390	3888	

Table S2 Saturated Vapor Pressure (SVP) (p_{ws}) of water as a function of temperature^{2,3}

T / °C	0	10	20	30	40	50
SVP / kPa	0.62	1.23	2.34	4.25	7.38	12.34

Considerations of the effect of RH changes on electrolyte in the microporous PTFE membranes

We have seen in the main text that the effect of changes in ambient %RH is to add or remove water from the electrolyte with corresponding increasing or decreasing electrolyte weights and volumes. However, the effects are not straightforward throughout the sensor.

If we look at the sensor structure of an electrolyte/membrane interface – Figure S2 – it can be seen that the electrolyte is shown as a thin film extending along the walls of the capillary beyond the meniscus.⁴ It will be shown below that the most dramatic changes in the electrolyte when exposed to different external RH values will be in those thin films.

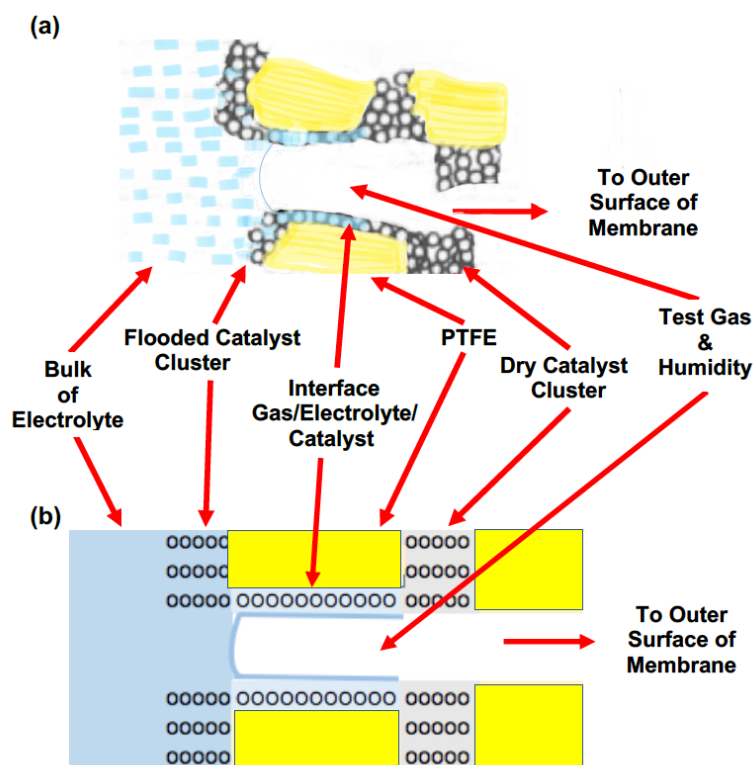


Figure S2(a) Model of a pore in a PTFE bonded high surface area electrocatalyst WE, based on Breiter.⁴ **(b)** Schematic of a pore in a gas membrane electrode

The transfer of environmental humidity throughout the sensor electrolyte is an intricate transport process, but we can get an approximate estimate of the time (t) required for it to occur in the electrolyte film in contact with the wall of a capillary in the membrane. It will be largely controlled by the slowest of the two mass transfer processes of diffusion of water vapor in air and water diffusion in the electrolyte film over the WE.

We have mentioned the relative rates of mass transfer in a sensor in the main text and that for each layer there will be an individual mass transfer coefficient. For the gaseous region through the gas entrance and gas space (Figure S1) the diffusion will be Fickian, and a typical diffusion coefficient (D_G) value for water vapor at 50°C will be 0.2 cm²s⁻¹ as calculated from the Chapman-Enskog equation.⁵ By consideration of the porous structure of the PTFE membranes used it can be shown that the Knudsen number Kn is ~ 0.5 , so transport is a mixture of Fickian and Knudsen diffusion and the effective diffusion coefficient (D_T) can be related to the separate coefficients (D_F and D_K) by

$$1/D_T \approx 1/D_K + 1/D_F \quad (S1)$$

with a typical value of ~ 0.04 cm²s⁻¹ for a compressed membrane with a tortuosity of ~ 1.5 . The value of D_G in the electrolyte at 50°C in 38% H₂SO₄ is 1.6×10^{-5} cm²s⁻¹; this can be obtained from the value in water at 50°C⁶ and by using the Einstein-Stokes equation with the viscosity for 38% H₂SO₄.⁷

Then the overall mass transfer coefficient (k_T) for the laminar structure can be described by the reciprocal sum of the individual mass transfer coefficients for the three zones: gas phase, (k_G), membrane (k_M) and electrolyte (k_E)

$$1/k_T \approx 1/k_G + 1/k_M + 1/k_E \quad (S2)$$

or

$$1/(D_T/L_T) \approx 1/(D_G/L_G) + 1/(D_M/L_M) + 1/(D_E/L_E) \quad (S3)$$

where L represents the corresponding diffusion lengths. With values of the coefficients given above and $L_G \sim 0.7$ cm, $L_M \sim 0.01$ cm, and $L_E \sim 0.3$ cm, we have

$$\begin{aligned} 1/k_T &\approx 1/(0.21/0.7) + 1/(0.04/0.01) + 1/(1.6 \times 10^{-5}/0.3) \\ &\approx 1/0.3 + 1/4 + 1/5.3 \times 10^{-5} \end{aligned}$$

It can be seen that the lowest mass transfer coefficient by far is that for the acid electrolyte film, so that will be the rate determining step in changing the acid concentration. Using the Einstein-Smoluchowski equation, the time for that to occur will be less than 1 ms.

Dilution changes the physical characteristics of the electrolyte and, in particular, the surface tension and viscosity. Let us consider a situation with 40% H₂SO₄ being diluted to 15% H₂SO₄, corresponding to 57%RH and 90%RH (cf. Figure 3, main text). At 25°C the surface tension changes from 76 mN m⁻¹ to 73 mN m⁻¹,⁹ and the viscosity from 2.5 mPa-s to 1.3 mPa-s.⁷ The lower surface tension will lead to a higher level of wetting on the walls of the membrane pores (cf. Figure S2) which will be assisted by the lower viscosity. The resulting greater electroactive area will lead to an enhancement of sensor output, which has been found experimentally.¹⁰

The bulk of the electrolyte at the base of the meniscus will eventually become diluted as well, and, as a result, it will increase in volume as it absorbs water. The free internal gas volume will decrease and when it approaches zero this can lead to electrolyte escape and leakage. This leakage with electrochemical gas sensors has been recognised for some time and has been discussed in a number of places;¹¹⁻¹³ one even mentions that pressure build-up can cause the sensing electrode to burst.¹³ Accordingly, account needs to be taken in sensor design of the maximum possible increase in volume for electrolyte expansion, to prevent leakage of electrolyte from the sensor; the acid electrolyte volume and concentration should be chosen to minimise the effect of ambient RH changing the electrolyte volume.

Temperature Dependence of %RH for H₂SO₄ Solutions

Table 2 in the paper (main text) shows that the values of %RH generated above H₂SO₄ solutions for a given acid concentration are only weakly dependent on temperature. This weak dependence is illustrated by the small variations in the values of the %RH values with temperature for each acid concentration as indicated by the 95% confidence intervals; Figure S3 shows it pictorially where the solid lines are the average zero-slope values in each case.

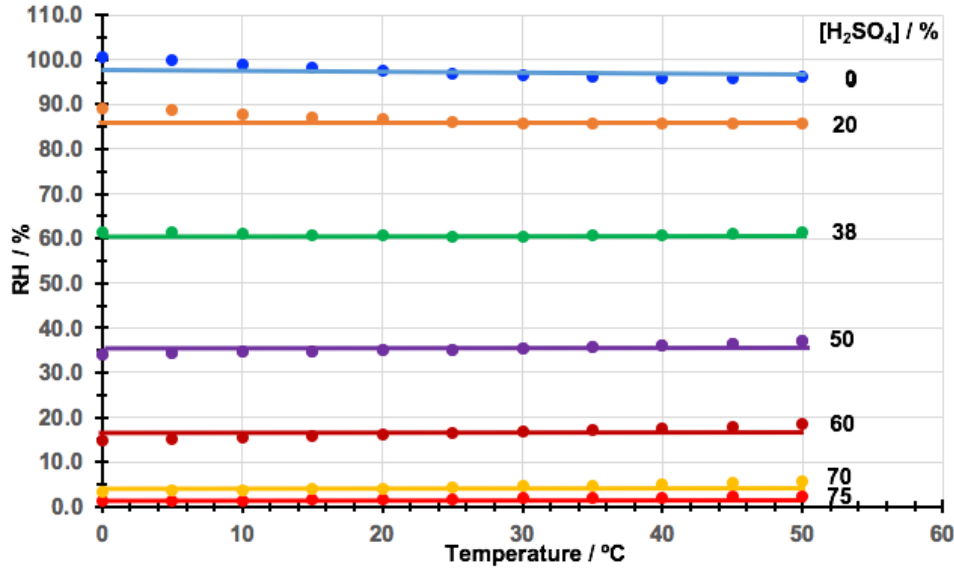


Figure S3 Plot of % RH generated by water over H₂SO₄ as a function of temperature

We now examine this behaviour, starting from the Clausius-Clapeyron equation,

$$d \ln p_w / dT = \Delta H_{vap} / RT^2 \quad (\text{S4})$$

where p_w is the water vapor pressure and ΔH_{vap} is the enthalpy of vaporization. In order to understand more fully the dependence of vapor pressure on temperature we need to integrate equation (S4) with appropriate integration limits; we assume ΔH_{vap} is constant, independent of temperature. We represent the upper pressure limit simply as p , which is the value for temperature T , and the lower limit as p^* with the corresponding temperature T^* , which can be referred to as the reference temperature, and is often taken as 273 K, or 0°C for convenience. Dropping the subscript *vap*, we obtain

$$\ln p - \ln p^* = -(\Delta H / R) (1/T - 1/T^*) \quad (\text{S5})$$

or

$$p = p^* \exp(-X) \quad (\text{S6})$$

where

$$X = (\Delta H / R) (1/T - 1/T^*) \quad (\text{S7})$$

Since %RH is defined as the ratio of the partial pressure of water vapor to the equilibrium vapor pressure of water at a given temperature (equation (4) main text), then for a particular sulfuric acid solution the generated RH can be obtained by the ratio of the acid water vapor pressure, p_{wa} , to the saturated vapor pressure of water, p_{ws} .

For the acid case we have

$$p_{wa} = p_{wa}^* \exp \{ -(\Delta H_{wa} / R) (1/T - 1/T^*) \} \quad (\text{S8})$$

or

$$p_{wa} = p_{wa}^* \exp \{ -(\Delta H_{wa} / RT^*) (T^*/T - 1) \} \quad (\text{S9})$$

Note that p_{wa}^* is not a function of temperature, but has a constant value corresponding to the reference temperature T^* ; the value will depend, though, on the acid concentration; cf. Table 1, main text.

For water we have

$$p_{ws} = p_{ws}^* \exp \left\{ - (\Delta H_{ws} / R) (1/T - 1/T^*) \right\} \quad (\text{S10})$$

or

$$p_{ws} = p_{ws}^* \exp \left\{ - (\Delta H_{ws} / RT^*) (T^*/T - 1) \right\} \quad (\text{S11})$$

where T will be the same as for the acid and we can choose T^* to also be the same reference point.

For a given temperature the %RH is the ratio of eqns. (S8) and (S10):

$$\%RH = 100 \times \frac{p_{wa}}{\bar{p}_{ws}} = 100 \times \frac{p_{wa}^* \exp \left\{ - (\Delta H_{wa} / R) (1/T - 1/T^*) \right\}}{p_{ws}^* \exp \left\{ - (\Delta H_{ws} / R) (1/T - 1/T^*) \right\}} \quad (\text{S12})$$

or

$$\%RH = 100 \times \frac{p_{wa}^*}{p_{ws}^*} \exp \left\{ - (\Delta H_{wa} - \Delta H_{ws}) / RT^* (T^*/T - 1) \right\} \quad (\text{S13})$$

It can be seen that in eqn. (S12) or (S13) the exponential argument is a function of T , just as for the separate partial pressures, so it is not immediately clear why the ratio of the partial pressures is weakly dependent on temperature. We will now examine the effect of the values of the various terms in the argument of the exponential.

We will examine eqn. (S11) for a reference temperature of 273 K and for temperatures in the range 273 K (0°C) and 323 K (50°C). Initially we determine the values for water of p_{ws}^* and ΔH_{ws} . Table S2 shows that the pressure at the reference temperature of 0°C (p_{ws}^*) is 0.62 kPa. If we plot the data for the full range 0°C to 50°C (Table S2) as $\ln p$ vs $1/T$ we can determine ΔH_{ws} – Figure S4.

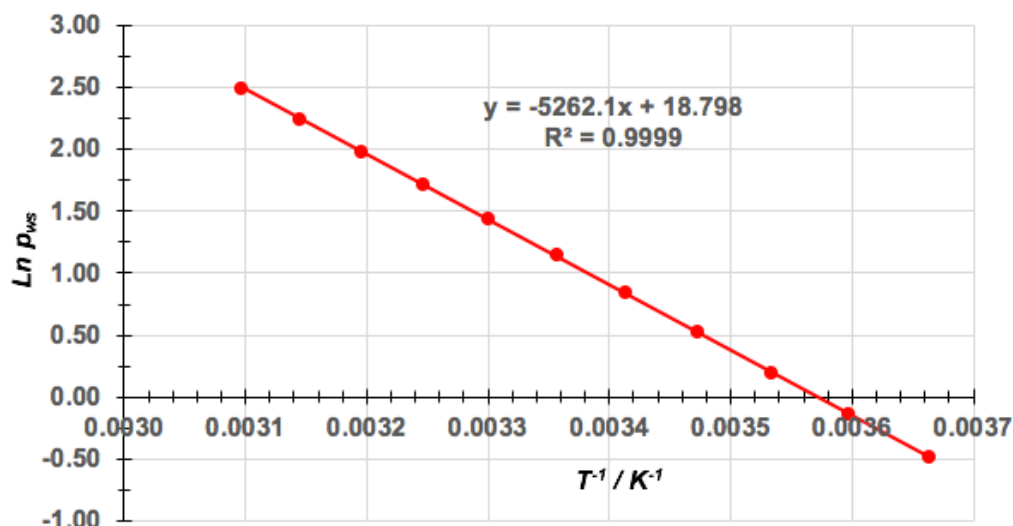


Figure S4 \ln saturated water vapour pressure as a function of reciprocal temperature

From the slope we can calculate $\Delta H_{ws} = 8.314 \times 5262 = 43.8 \text{ kJ mol}^{-1}$. We now need to do the same for each of the acid concentrations between 0% and 75%, but we will restrict the determinations of p_{wa}^* and ΔH_{wa} to selected concentrations – 10% 30%, 50%, and 70%. Figure S5 shows a typical plot; all the other plots have $R^2 = 1.0$.

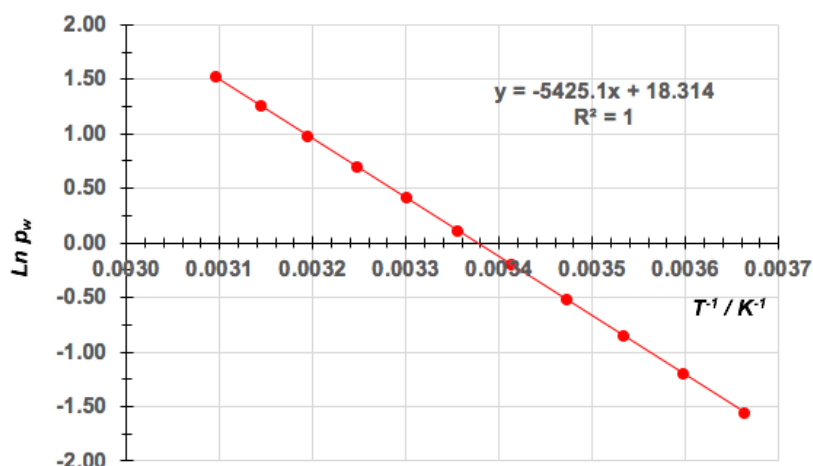


Figure S5 Ln water vapour pressure as a function of reciprocal temperature for 50% acid

Table S3 summarises the values of p_{ws}^* and ΔH_{ws} , and of p_{wa}^* and ΔH_{wa} for the selected acid strengths.

Table S3 Values of p_{ws}^* and ΔH_{ws} , and of p_{wa}^* and ΔH_{wa} for the selected acid strengths

Water	p_{ws}^* / kPa	$\Delta H_{ws} / \text{kJ mol}^{-1}$
	0.62	43.8
[Acid] / %	p_{wa}^* / kPa	$\Delta H_{wa} / \text{kJ mol}^{-1}$
10	0.60	43.2
30	0.47	43.5
50	0.21	45.1
70	0.02	51.7

And Table S4 gives the corresponding values of %RH calculated using eqn. (S13) for five temperatures in the range 0°C to 50°C.

Table S4 %RH values for selected acid strengths and temperatures

Temp / °C	[Acid] / %			
	10	30	50	70
0	96.7	76.0	34.2	3.2
10	96.0	75.7	34.9	3.7
20	95.3	75.4	35.6	4.1
35	94.3	75.0	36.6	4.8
50	93.5	74.6	37.5	5.6
Mean	95.2±2.1	75.3±0.9	35.8±2.2	4.3±1.5
Mean Table 2	93.7±1.1	74.2±0.7	35.4±0.6	4.4±0.5
% p_{wa}^*/p_{ws}^*	96.8	75.8	33.9	3.2

The weak temperature dependence of %RH commented on above is also clearly seen from the data in this table; the errors are the 95% confidence intervals. There is reasonable agreement with the averages for %RH values directly calculated using the Greenwalt equation for partial water vapour pressures over acid solutions - Table S1. One might think the agreement is not too surprising since we are using the same source data, except that

we have used an equation here that clearly shows that %RH should have a temperature dependence. However, if the exponential term in that equation were always to have a small value of the argument then the term will have a value close to unity. In fact, we can see that this is the case because the ratios of the two partial pressures (p_{wa}^*/p_{ws}^*) of the pre-exponential term agree reasonably with the values from the full expression.

As noted earlier, the agreement is less good as the acid concentration increases above 70%, but at that point the relative humidity is so low that the absolute values are not significant.

In conclusion, therefore, there is no fundamental reason for the weakly dependent behaviour of %RH with temperature and it simply arises from the numerical values of the parameters in the derived equation for %RH. When there is a greater dependence at higher acid concentrations the absolute values of %RH are so small that their temperature dependence is negligible.

Densities for Different %H₂SO₄ Solutions as a Function of Temperature

Figure S6 shows plots of density as a function of %H₂SO₄ for three different temperatures, 0°C, 20°C and 50°C based on published data.¹⁴ With the equations given for quadratic fits in each case the fit is good, and using the equations to calculate density values gives agreement with published data to better than $\pm 0.5\%$.

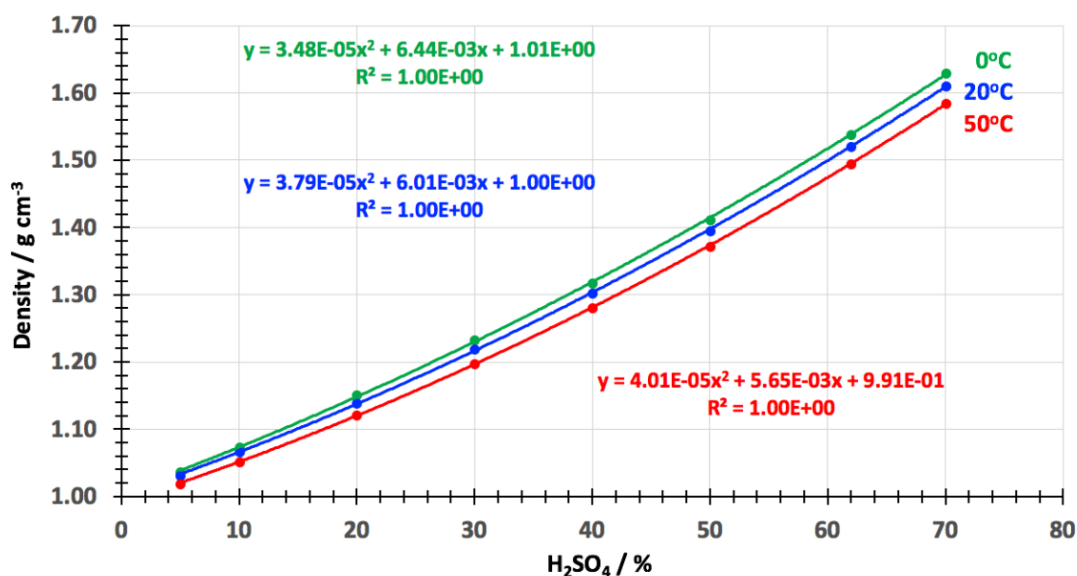


Figure S6 Density of %H₂SO₄ solutions at 0°C, 20°C and 50°C

REFERENCES

- (1) Greenewalt, C.H. Partial pressure of water out of aqueous solutions of sulfuric acid. *Ind & Eng Chem.* **1925**, *17*, 522-523.
- (2) Huang, J. A simple accurate formula for calculating saturation vapor pressure of water and ice. *J. Appl. Meteor. Climatol.* **2018**, *57*, 1265–1272. (b)
- (3) https://en.wikipedia.org/wiki/Vapour_pressure_of_water.
- (4) Breiter, M.W. *Electrochemical Processes in Fuel Cells*, Springer-Verlag, Berlin, 1969.
- (5) https://en.wikipedia.org/wiki/Mass_diffusivity.
- (6) Holz, M; Heila, S.R.; Sacco, A. Temperature-dependent self-diffusion coefficients of water and six selected molecular liquids for calibration in accurate 1H NMR PFG measurements, *Phys. Chem. Chem. Phys.* **2000**, *2*, 4740-4742.
- (7) Rhodes, F.H.; Barbour, C.B. The viscosities of mixtures of sulfuric acid and water, *Ind Eng Chem.* **1923**, *15*, 850-852.

- (8) Liu, S; Li, S. Liu, J. Jurin's law revisited: Exact meniscus shape and column height. *Eur. Phys. J. E.* **2018**, 41: 46.
- (9) Suggitt, R.M.; Aziz, P.M.; Wetmore, F.E.W. The Surface Tension of Aqueous Sulfuric Acid Solutions at 25°C, *J. Am. Chem. Soc.* **1949**, 71 676-678.
- (10) Wei, P.; Ning, Z.; Ye, S.; Sun, L.; et al. Impact analysis of temperature and humidity conditions on electrochemical sensor response in ambient air quality monitoring, *Sensors*, **2018**, 18, 59; doi:10.3390/s18020059
- (11) Chan-Henry, R.Y. Design and development of electrochemical gas sensors, *PhD Thesis*, City University London, **1992**
- (12) Aston, W.J.; Chan, Y.S. Electrochemical gas sensor, *US Patent*, 5,395,507, **1995**.
- (13) Mole, T.J. Method of manufacturing an electrochemical gas sensor, *European Patent*, EP 1 366 355 B1. **2014**.
- (14) Lide, D.R. (Ed), *Handbook of Chemistry and Physics*, 9th Edition, Internet Version **2010**, Section 15_25_86.